ILASS–Europe 2017, 28th Conference on Liquid Atomization and Spray Systems, 6-8 September 2017, Valencia, Spain
http://dx.doi.org/10.4995/ILASS2017.2017.4600

Investigation of the effects of domain representation and boundary condition selection in numerical simulations of micro scale flows with phase change

Daniel Pearce*[1], Konstantina Vogiatzaki[2],A.M.K.P Taylor[3],Y. Hardalupas[3]
[1]Delphi Diesel Systems Ltd, Imperial College, London,UK
[2]Advanced Engineering Center, University of Brighton, UK
[3]Mechanical Engineering Department, Imperial College, London, UK
*Corresponding author: Daniel.Pearce@delphi.com

Abstract
Cavitation is a phenomenon affected considerably by the underlying pressure waves that occur on similar time and length scales as the bubble dynamics. Thus appropriate representation of wave dynamics within numerical frameworks is of paramount importance for the prediction of the phase change process in the nozzle as well as the subsequent spray formation. In this paper we focus on investigating the sensitivity of the wave dynamics within a compressible Large Eddy Simulation framework with regards to downstream geometry and boundary representation. Diesel was used as working fluid and was injected at various pressures through a micro-channel. Results in terms of vapour fraction, velocity and pressure are compared with the experimental data of Winklhofer [30,31]. The downstream domain length and reflectivity properties are shown to exert a significant effect on in-nozzle processes.

Keywords
cavitation, LES, pressure waves, OpenFOAM

Introduction

The term cavitation is used to describe the phenomenon of vapour production within a homogeneous liquid due to the pressure reduction below the vapour pressure of the liquid. Dynamically occurring cavitation arises when the local flow conditions are such that the fluid detaches from a wall (sometimes at a "salient point" such as a corner) and if the associated streamline curvature is sufficiently small, low pressure regions are formed on the surface as in propellers, hydrofoils *etc*. A different mechanism can arise in orifices and nozzles, where the high speed flow through the throat causes - essentially according to Bernoulli's theorem - so that this local low pressure arises far from walls and cavitation is generated within the stream. An example of the latter cavitation is Craya-Curtet co-flowing, confined jets where the entrainment rate may be strong enough to generate pressures below the vapour pressure and hence cavitate [3]. A more comprehensive review of the various forms of cavitation may be found in Franc [12], Bergant [4], Dumont [6] and Arndt [2,3].

In the present study, we examine cavitation as it occurs within micro channels, particularly those used as a simplified approximation for a nozzle. Nozzles are fundamental to a wide range of industrial processes such as spray painting, jet cutting and fuel injection systems. This application was chosen for a number of reasons: the geometry is simple and experiments for which measurements are available such as Winklhofer *et al.* [31] or Mauger *et al.* [18], the problem is of commercial interest (e.g. to support emissions regulations) and there exists a wide body of previous studies upon which to build. The specific difficulties around the conditions found in typical injection systems may also be seen as an extreme case with which a numerical modelling scheme would need to cope. This flow has also, therefore, a wider field of application to the more general problem of numerical simulation of hydrodynamic cavitating flows.

In this paper we asses the predictive capabilities of a numerical framework within the Large Eddy Simulation context when Diesel fuel is injected at various downstream pressures through a micro-channel. In particular, the aim was to improve model behaviour in the occurrence of critical cavitation and beyond. Critical cavitation is defined as the point at which the flow ceases to be dependent on the driving pressure difference and has reached a maximum mass flow rate (known as 'choked' conditions). If the pressure difference is greater than that required for choked conditions, the cavitation region may cover the full spanwise extent of the channel and be 'fully choked'. This flow regime between choked and fully choked is currently poorly reproduced by simulation in the literature. To address this poor understanding, the transient nozzle exit pressure was identified as the focus for investigations. Thus, in order to correctly model the processes within the nozzle, the nozzle exit pressure and its relationship to the farfield pressure were explored. Since it is difficult experimentally to measure the pressure *at* the nozzle exit, typically it is the mean value of the *farfield* pressure that is reported instead. The novelty of this paper is to investigate this discrepancy between experimentally measured downstream pressure and its correct representation in terms of model parameters. For a model to be validated against such experimental pressure data therefore, the downstream

domain must contain the relevant features that affect this pressure. From this, the downstream length and boundary condition were varied parametrically. The second feature of importance is the presence of pressure waves in the domain which can substantially change the nozzle exit pressure in a time dependent way. For these reasons, the experimental data for pressure at a measured downstream station were compared to different pressure values of both fixed and non-reflective (wave transmitting) domain terminations in order to attempt to replicate the correct conditions at the nozzle exit.

The structure is as follows: We first present our numerical framework as well as the experimental data source. We explain in detail the important sub-models used (phase change, turbulence and compressibility) as well as the numerical parameters that affect the results (physical properties, grid and boundary conditions). A sensitivity analysis for all the aforementioned models and parameters is not possible here due to space limitations. Thus, in the result section, we chose to present the sensitivity of the predictions to the selection of pressure boundary conditions that are not well represented in the literature up to date. We present the numerical results in terms of void fraction, velocity and pressure and we compare these with the corresponding experimental data [31].

Experimental Setup

The simulations in this work are compared to experiments described in [31] and the model nozzle is shown in Fig. 1. Diesel fuel was pumped through a micro channel eroded into a 0.3 mm thick steel sheet which was sandwiched between two sapphire windows, allowing the visualisation of the channel and forming a nozzle-like structure. The geometry analysed here corresponds to the throttle geometry called "U" in [31], which is a rectangular shaped channel of 100 x 301 x 284 mm with an inlet radius of 20μm. The channel extended 10mm upstream and downstream of the nozzle to minimise the effect of the boundary conditions within the nozzle. In all of the experimental cases, the upstream pressure was 100bar, and the outlet pressure was varied.

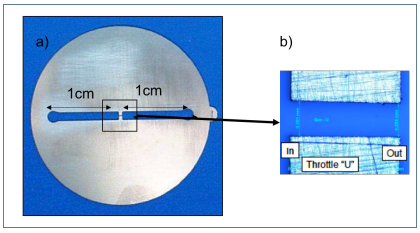

Figure 1. (a) View of the experimental nozzle (b) Zoom-in in throttle geometry U. [31]

Numerical Parameters

In this work, OpenFOAM [11] was chosen as the code base due to its extensible nature with access to the source code in order to create and modify the governing numerics. A brief description of the governing equations, phase change, turbulence and compressibility sub-models as well as grid specifics are presented in the following section. Special focus is given to the choice of the boundary conditions, that is the main topic of this work.

Multiphase modelling including compressibility

For the simulation of the two phases present (fuel vapour and liquid fuel) in the domain we are using the so called "one-fluid approach" within a compressible framework. Instead of having an individual set of transport equations for each phase, in every computational cell liquid and vapour are treated as a single continuum. The compressibilities of both phases are taken into account and the temperature is assumed to be uniform. The one fluid approach is suitable for problems where the second phase may be considered to be fully dispersed within the first such as 'cloud cavitation' or strongly turbulent cavitation of numerous small, discrete bubbles. It is less well suited to slug flow or stratified flow situations where the two phases might reasonably be expected to have differing velocities. In our case, and given the high pressure differences for the geometry under consideration, this approach can be considered as a reasonable assumption and has been validated previously by authors such as Salvador *et al.* [25]. The starting point of forming the numerical framework used is the following equation of continuity

$$\frac{D\overline{\rho}}{Dt} = \psi \frac{D\overline{\rho}}{Dt} \tag{1}$$

which is based on a barotropic equation of state. The term ψ is the compressibility of the mixture which is defined as $\psi = 1/c^2$ (where c is the speed of sound) and needs to be determined. Equation 1 can be used either directly in the continuity equation to formulate a pressure equation, or integrated to obtain the pressure as a function of the density as suggested by Schmidt *et al.* [26]. In our case we use the former approach, following [14]. We use the notation with bars over the quantities since the framework is formulated within the LES context. The equation of state for the mixture should then be consistent with the liquid and the vapour equations of state, both at the limits

when there is pure liquid or pure vapour, and also at the intermediate states when there is a mixture. The densities of the two phases are defined as:

$$\overline{\rho}_v = \psi_v \overline{p} \quad \text{and} \quad \overline{\rho}_l = \overline{\rho}_l^0 + \psi_l \overline{p} \tag{2}$$

The terms ψ_v and ψ_l are the compressibility factors of vapour and liquid respectively. In order to separate the amount of volume that each phase occupies in this "mixture" fluid a phase indicator function known as the vapour fraction, α, is used. α is defined as

$$\overline{\alpha} = \frac{\overline{\rho} - \overline{\rho}_{lsat}}{\overline{\rho}_{vsat} - \overline{\rho}_{lsat}} \quad \text{where} \quad \overline{\rho}_{vsat} = \psi_v \overline{p}_{sat} \tag{3}$$

It can be seen that if there is no cavitation within a cell then $\overline{\rho} = \overline{\rho}_{lsat}$ resulting in α =0 while for the case that a cell is full of vapour $\overline{\rho} = \overline{\rho}_{vsat}$ and α=1. The equilibrium model as described above has as its main advantage its simplicity. There is no need to solve an additional transport equation for the vapour volume fraction, since the fluid above the vapour pressure is defined as a liquid, the fluid below the vapour pressure as vapour and the change of density with pressure is defined by an equation of state. Moreover, since it is based on local equilibrium assumption it ignores the effect of the interfacial forces between different phases and thus the surface tension term in the momentum equation is considered negligible. Models of this category are more appropriate for high speed nozzle flows in that the effect of surface tension is minimised resulting in an homogeneous mixture of bubbles and liquid in each cell such as in diesel fuel injectors [7]. The model has been compared with alternative models accounting for interfacial forces in our previous work [27] for various cavitation numbers but for a larger scale geometry (lower velocity) and results indicated a similar behaviour of the two models as the cavitation number was increasing. The choice of an appropriate closure relation was studied by Gonclaves and Patella [8] using a one fluid model applied to a venturi geometry. This combined a stiffened gas model with the barotropic model, described above, using a compressible RANS solver. They used a sinusoidal form of the gas closure relation which gave a smooth transition between pure liquid and pure vapour speed of sound (and hence compressibility) but this may be unphysical since it is known that the speed of sound in a mixture can be significantly *less* than that in either of the two phases individually.
Combining Eqs. 2,3 we form the mixture's equilibrium equation of state.

$$\overline{\rho} = (1-\alpha)\overline{\rho}_l^0 + [\alpha\psi_v + (1-\alpha)\psi_l]p_{sat} + \psi(p - p_{sat}) \tag{4}$$

The equations of motion are then closed with the constitutive relations for the density, ρ , the dynamic viscosity (using a linear model), μ and the compressibility ψ.

Compressibility and Thermophysical properties

A linear model for compressibility was used since it is considered more consistent with the volume of fluid method, where viscosity and mass fraction are similarly described by linear equations [14].

$$\overline{\psi} = \alpha\overline{\psi}_v + (1-\alpha)\overline{\psi}_l \tag{5}$$

When Eq.5 is used, then the equation of state for the liquid can be reduced to a linear equation as well with $\overline{\rho}_{l,vap} = \rho_{l,sat} + \psi_p$. Alternative models are the Chung [5] and the Wallis model [28]. Literature [13] suggests that the Wallis model represents the lower speed of sound (compressibility) in a bubbly mixture in a more physical way, but it is rather unstable when used for high speed flows.

In terms of the choice of the individual compressibility factors ψ_l and ψ_v the physical properties of the diesel fuel have to be considered. The difficulty in the use of Diesel in numerical simulations is that the fuel typically varies seasonally as well as geographically so its properties are generally defined in terms of a range rather than a specific value. For example in Europe, the specification of common pump diesel must conform to EN590 [1] (which is more concerned with sulfur content and biofuel components due to their effect on emissions) so that the stated density must be between 820 and 845 kg/m^3. Koukouvinis *et al.* [15] chose to use a value well outside this range, presumably in order to tune their model and reduce the propensity of the code to develop significant negative pressures. Habchi *et al.* [9] also chose a value outside the EN590 range from some of their earlier work on lumped parameter modelling [10] which was focused on vaporisation rates and simulating spray conditions at 400K. The selection of subcomponents and use of a gas derived equation of state may explain this lower than usual density value. All other authors reviewed chose values close to the EN590 range but it is generally unclear whether this is for convenience or whether it served to help drive model outputs. For the current simulations the thermodynamic properties in Table 1 have been adopted.

Turbulence and the Sub - Grid scales

Turbulence in the context of small scale , high speed flow is difficult to interpret within the realm of multiphase flows since not only are the mechanisms poorly understood [23] but the transition to fully developed turbulent flow, which might be expected as the Reynolds number increases, can be delayed significantly. Established vapour regions near the wall can reduce the effective viscosity and associated frictional losses such that the central jet can persist in a turbulent transition regime for a wide range of pressure differences. In this study, therefore, a transient methodology is required (LES) even though the problem is quasi-steady state. It should be noticed that one of the difficulties in performing LES in the context of cavitation is that it is hard to determine the length scale spectrum and the resolution requirements. Although in single phase flows the smallest scale is defined through the Kolmogorov scale, in two phase flows the definition of an equivalent scale is difficult. In the current work we model the sub-grid tensor term with an algebraic eddy viscosity models in which the stress tensor τ_{ij}^{sgs} is related to the resolved strain rate tensor $\widetilde{S}_{ij}$ by means of a scalar eddy viscosity given by an algebraic equation. It is based on the Boussinesq hypothesis associating τ_{ij}^{sgs} with a sub-grid scale (sgs) turbulent viscosity, μ_T. The idea is that the momentum transfer caused by turbulent eddies can be modelled with an eddy viscosity in the same way the momentum transfer caused by the molecular motion in a gas can be described by a molecular viscosity. The model is known as the Wall-Adapting Local Eddy-viscosity model (WALE) [19]. The sgs viscosity is dynamically computed with the square of the velocity gradient tensor rather than the resolved strain rate used in Smagorinsky-type models. This velocity tensor can not only account for the effects of both strain and rotation rate of the smallest resolved turbulence fluctuations, but also recovers the proper near-wall scaling for the eddy viscosity without requiring dynamic procedures. Moreover, as the WALE model is invariant to any coordinate translation or rotation and no test-filtering operation is needed, it is therefore well suited for LES in complex geometries [19].

Boundary conditions

In the course of reviewing existing literature on the simulation of cavitating channels, it was found that there exists a dearth of information on the downstream length requirements of placing the exit boundary condition in order to correctly satisfy a pressure governed boundary condition. Previous authors have assumed (implicitly) that the pressure at the nozzle exit is the same as that found downstream and thus experimental values are often applied at unphysical domain locations (e.g an experimental value from a sensor distant from the nozzle is applied at the nozzle exit). This is done to reduce the computational domain and hence computational cost. In the experiments of Winklhofer, fuel pressure levels are measured 35 mm upstream and downstream of the observation element. This will be referred for the rest of the paper as "P_{out}" (the real physical outlet) while the pressure used in the numerical simulations as "$P_{boundary}$". These two pressures do not necessarily coincide even if the same case is under consideration since "$P_{boundary}$" is dependent on the size of the simulated geometry that imposes a specific pressure drop in between the exit of the nozzle and the experimentally measured boundary condition of the domain. It may also allow different levels of pressure wave reflection. It should also be noted that, in the experiment, the gauge used may be damped in order to observe a smooth value for monitoring purposes. Even with a high frequency pressure sensor, the reported values have lost the richness of the full signal content which would have been an indicator of the frequency and amplitude of any transient fluctuations. "P_{out}" should then be considered to be time averaged with the possible existence of an unknown fluctuating component. Examples of zero downstream length include [29], [20] and [17] while those classified as 'short' -between 1-5 diameters include [15] while [22] utilise larger exit domains with extra geometrical features. In this study, we consider the effects of the downstream length to the exit boundary of the computational domain by varying the distance from the outlet of the channel section to the boundary by 5, 9 and 12mm (keeping in mind that the channel length is 1mm while the length of the geometry before the nozzle is also simulated as 1 mm).Thus, the 12mm long case essentially represents the size of the downstream experimental geometry closely. One additional case with 3mm length was tested: however it is not reported here since the close proximity of the exit boundary to the nozzle outlet led to considerable numerical instabilities.

The boundary conditions were treated as a total pressure condition at the inlet to the domain with a small component of turbulent kinetic energy and negligible velocity. For the the outlet boundary condition, two conditions were tested. The first configuration is typical for this type of problem and uses a fixed value condition (FP) imposed as a pressure constraint to ensure that the equations are well bounded. This type of problem is the classic 'pressure driven flow' scenario in which the velocity at the domain exit is considered to be a dependant variable. The second configuration tested was a novel variant of the pressure wave transmissive (PWT) condition that was modified to be compatible for multiphase problems. The PWT condition attempts to transmit all incident pressure waves outside the domain and maintain a given far field value of pressure. This is done by attempting to keep the instantaneous value 'close' to the given far field value. Here, 'close' is defined by a separate parameter, the far field distance. A smaller far field distance implies that a smaller deviation is allowed from its prescribed value whilst a larger far field distance allows greater deviation. The core scheme for this is derived from Poinsot and Lele [21] and is accomplishing by assuming

Table 1. Thermodynamic properties of Diesel

$p_{sat}(Pa)$	$\rho_{l,sat}$ (kg/m^3)	$\rho_{v,sat}$ (kg/m^3)	ψ_l	ψ_v
5400	832	0.1361	0.0000005	0.0000025

that, for high Reynolds flows, the hyperbolic part of the Navier Stokes equations represent the wave component of the local pressure field.

Grid

The cell size in the nozzle, that is the area of interest, is 0.02mm while outside the nozzle it is 0.06mm. The Reynolds numbers considered for all three outlet pressure cases (15bar, 30bar, 50bar) is of the order of 10^6 while the Taylor scale is of the order of 0.001mm. The total number of cells was varied depending the size of the geometry in order to maintain a constant resolution. The near wall region was resolved to typical values of $y^+$of the order 1-5 such that the LES terms are considered to be implicit. To ensure a stable solution, transient calculations with a step of 250 μs were performed. The convergence criteria used for the calculations are based on the values of the residuals (which have to reach a value of 10^{-7}, at least, for all equations) and the mass flow rate (which has to be stabilized as much as possible). The time step is limited by both the Courant number (taken as 0.2) and the acoustic Courant number (taken as 12).

Results

Figure 2 shows the vapour fraction, pressure and velocity instantaneous fields for the 5mm domain geometry at time t=0.075ms using FP boundary conditions. Three different outlet pressure values are presented. Looking at the α profiles it can be seen that as the outlet pressure is increased, the amount of vapour within the nozzle reduces and this is comparable with the experimental observations [31]. Also, although a structure resembling a cavitation cloud is evident after the nozzle exit for $P_{boundary}$ = 15bar, this disappears for higher pressures. Looking at the velocity and pressure plots (especially at the area downstream of the nozzle), it can be seen that using a FP boundary condition leads to 'pulses' in the jet velocity with alternating fast and slow regions with similar vector directions, implying that the rotation is low and there is no significant reverse flow. This spatial oscillation of the velocity magnitude has several implications for the overall flow structures that may be observed. We suggest that these velocity fluctuations are a result of the pressure waves trapped in the domain reflecting and interacting at nodal points so local high and low pressure regions act to retard or accelerate the jet as it moves away from the nozzle. The challenge that arises in numerical simulations using FP boundary conditions is that there is no straight forward way to separate pressure waves associated with the pressure outlet conditions and pressure waves that occur "naturally" because of the nozzle operating conditions. By considering a PWT boundary condition as we suggest in this work, we have the potential to better control of the waves that are allowed to reflect within the domain and thus help us separate which phenomena are associated with naturally occurring waves and which ones are related to numerical artefacts
One implication relevant to pressure prediction that is evident from the plots of Fig. 2 is that local pressure differences in streamwise sections of the downstream domain drive velocity profile differences in the shear layer which in turn affect local low pressure regions in which cavitation is likely. It is interesting to note that an examination of the vorticity associated with this flow shows very little correlation and no clear vortical structures could be observed. The pressure and velocity plots in Fig. 2 have additional black contours added to highlight those areas where the pressure is less than the vapour pressure. Cavitation is not observed for the 55bar outlet pressure case and only observed in the region of the vena contracta for the 30bar case. The 30bar velocity plot shows how the jet shear layer undergoes velocity differences along the jet centreline while the 15bar velocity plot shows how greater pressure differences can lead to vapour formation in the shear layer. It is evident that correct prediction of the pressure waves in the domain is an important factor in the overall solution.
Another implication is that the variable pressure difference across the nozzle due to these wave effects can lead to instabilities in the cavitation which is generated in the usual vena contracta regions and along the nozzle walls. Supercavitation is partially suppressed and the vapour along the nozzle walls may not always extend fully to the exit with small backflow into the channel as the local pressure at the exit corner is higher than the vapour pressure. The momentum of the jet inside the nozzle is high enough that the boundary between the fast moving fluid and the near static vapour is essentially fixed after the initial jet acceleration.
An additional important remark from these plots is relevant to the cavitation evolution in the nozzle for the 30bar exit pressure that is identified in the experiments as the critical cavitation case (see Fig 3). The experimental data indicates that cavitation and the subsequent 'bubbly' mixture could extend over the entire spanwise section of the channel as critical cavitation pressure differentials are exceeded. For the U geometry, this evolution occurs rapidly after the exit pressure is reduced below 30bar, as even the 29bar exit pressure condition has substantially increased cavitation probability. This could explain why that the simulated 30bar FP case (seen in Fig. 2), which is particularly close to a high sensitivity region, shows a low cavitation region within the nozzle.
In order to better understand the effect of pressure waves within the domain, the wave transmissive boundary condition is applied at the outlet. This configuration was tested at 20bar far field pressure with 5, 9 and 18mm far field distance values. Although with this approach waves are able to exit the domain as expected, (in theory limiting the effect of artificial pressure oscillations), some pressure variations are still present because of the high Reynolds number of the flow. These instabilities interact with the vapour fraction leading to vapour collapse events in the downstream area. These collapse events trigger pressure waves which are then able to travel upstream towards the nozzle in a similar way as that which occurs in the experiment. We first zoom into the nozzle cavitation development for the 15bar FP case and 20bar PWT (see Fig. 4). The experimental evidence [31] is that under these conditions the cavitation should extend to the nozzle centreline leading to fully choked conditions (as in Fig 3b). In our simulations we can also see some indication of the cavitation regions beginning to close on the centreline for the FP conditions with instabilities growing in the phase transition region, something that is largely missing from other

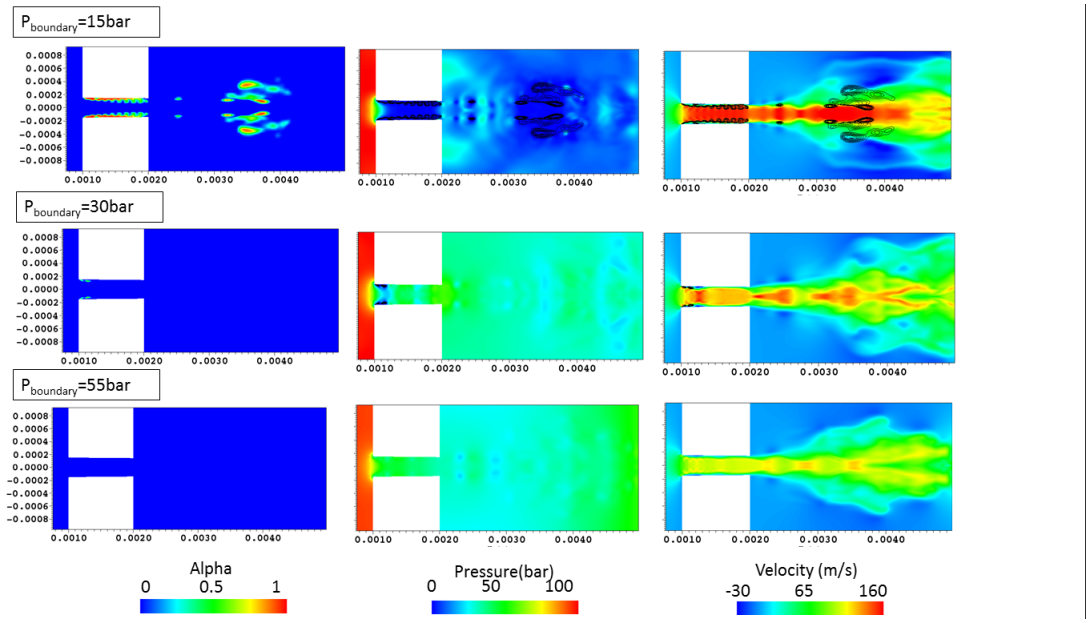

Figure 2. Instantaneous contour plots of vapour fraction, pressure and axial velocity at t=.075s. Boundary condition is considered as fixed pressure. Axis scale is m.

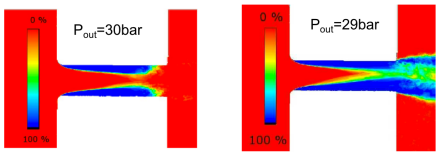

Figure 3. Experimental cavitation probability at critical cavitation point and beyond [31].

simulations of similar geometries. In contrast it can be noted that as the pressure waves are allowed to escape the domain, the cavitation in the PWT case lacks any turbulent features and more closely resembles lower pressure cases. This highlights the impact that reflections from the boundary (either physical or artificial) have on the nozzle cavitation regime. Previous work such as [16] and [24], for example, have examined the same geometry but have not addressed this issue, i.e that fully choked flow conditions are met. In contrast in Fig. 4 we can see that when waves are allowed to travel back to the domain then the framework is better capable of representing some of the important features. Of course further understanding is needed since the waves in the case of FP are more relevant to the length of the domain rather than the actual present in the domain because of the injection conditions. In previous work of [14], in order to increase the amount of vapour within the nozzle the upper and lower walls were considered with a slip condition for the velocity, similar to that used in supersonic compressible flow. This was done under the assumption that a no-slip boundary condition would lead to overestimates of the thickness of the boundary layer, resulting in strong vortices in the centre of the channel and incorrect modelling of the flow's cavitation. The assumption of a slip condition seems rather unphysical and according to our observations, a re-examination of the boundary conditions might be more appropriate.

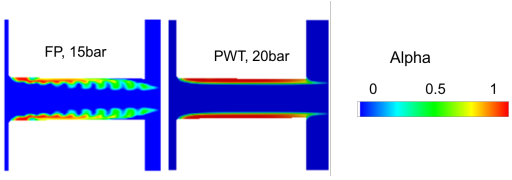

Figure 4. Vapour fraction in nozzle region, Left: 15bar FP, $5mm$ downstream length. Right 20bar PWT, far field $5mm$

Figure 5 shows a comparison of the pressure profiles along the centreline of the nozzle for a selection of the tested configurations. The experimental profile inside the nozzle is characterised by an initial pressure drop because of the flow turn at the inlet as well as a sudden pressure rise at around $0.5mm$ downstream. It can be seen that for the 15bar cases where FP conditions are used, only the case of $5mm$ captures the correct behaviour. This does not necessarily mean that this boundary condition is accurate. It indicates only that since we have set the boundary $5mm$ downstream the exit of the nozzle and this specific boundary imposes reflection of pressure waves, these

waves travelled back upstream inside the nozzle recovering some of the behaviour present in experiments. For the other two cases (9mm and 12mm), that in reality are closer to the real experimental geometry, the pressure drop is over-predicted inside the nozzle. The pressure only partially recovers because of the pressure increase at the exit. These results are similar to previous studies in the literature [13]. Looking at the poor agreement of the prediction of the 9mm and the 12mm case even downstream of the nozzle exit (at 1.5mm), one can argue that since we impose 15bar pressure at 9mm and 12mm boundary we cannot really predict accurately the pressure difference measured by the experiment at 35mm downstream of the nozzle. In an effort to better tune our results, we include the results of a 9mm geometry with $P_{boundary}$=20bar. We can see that with this re-adjustment although the results match better at 1.5mm, the predictions inside the nozzle are still poor. Changing the boundary to wave transmissive conditions gives two important advantages. One is that for both the 5mm far field and the 18mm far field values, part of the in nozzle pressure profile is correctly recovered. Moreover, with this method, the size of the simulated geometry is not changed (this is always 5mm): instead the far field parameter is controlled and hence so is the amount of waves allowed within the domain. This considerably reduces the computational cost in comparison to FP conditions in which the geometry was varied in order to control the boundary response.

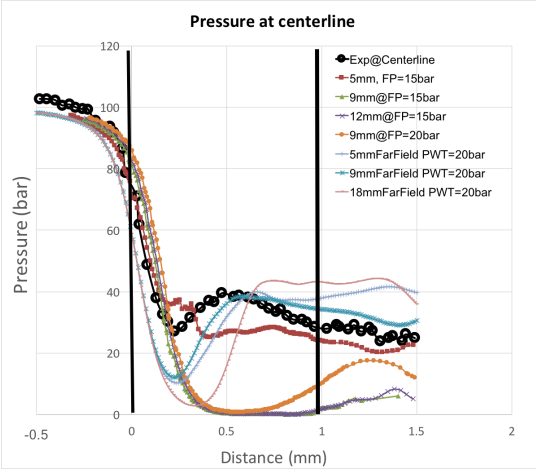

Figure 5. Pressure profiles along nozzle centreline comparing experimental data at 30bar to various downstream pressure values

Figure 6 shows the spanwise velocity profiles for the 15bar experimental condition at x=0.17mm. Five numerical cases are considered (three with FP boundaries and two with PWT). The experimental data shows a peak in velocity towards the nozzle upper and lower boundaries which is indicative of the lower viscosity and hence frictional losses in this area because of cavitation. It also shows a recovery of the velocity in the nozzle core although it does not achieve a maximum. The 15bar, 5mm downstream FP case is best able to reproduce this result although it does not show the higher central area. The PWT condition shows a flatter profile which indicates that the shape of the FP conditions is being influenced by wave reflections present in the downstream area. The wave transmissive cases also demonstrate the differences seen across the various far field values that were used. Figure 6 has far field values of 5mm and 9mm, all at the same $P_{boundary}$ of 20bar. A linear trend in the maximum velocity as the far field values increase can be seen. Note that the 9mm case with FP and the 9mm PWT both at 20 bar predict similar velocity magnitude at the centerline but they differ in the prediction at the layer closer to the wall. This can be considered as an indication that capturing the pressure waves better within the domain is not expected to change substantially the main jet behaviour but it is expected to change the cavitation predictions. Further variations of the wave transmissive case are currently running in order to better explore this relationship although they were not available at the time of writing.

Conclusions

The downstream boundary conditions of a micro-channel geometry with in nozzle cavitation at critical cavitation and fully choked flow conditions were examined through numerical experiment and their impact assessed. The domain bounds and definition have been shown to be an area poorly understood with regards to their effect on in nozzle results. Using rigid exit conditions mean that pressure waves generated either within the nozzle or the downstream domain are reflected and continue to influence the local flow conditions. Downstream domain length and choice of boundary condition are therefore important in order to accurately model the pressure field and cavitation within the nozzle. The outlet from the nozzle section is prone to external cavitation in the shear layer (for choked flow conditions) which can also impact the nozzle exit pressure, particularly when attempting to validate against experimental results where the downstream pressure may be measured at a location some distance from the nozzle itself. It was found that vorticity (especially for cavitation developed outside the nozzle) did not play a large part in external cavitation formation, rather the velocity difference in the shear zone interacting with pressure waves had the greatest influence. A novel wave transmissive boundary condition for multiphase flow was tested and shown to be promising in replicating in-nozzle pressure profiles compared to more traditional fixed boundary conditions. However it as proved less accurate in replicating the velocity profile close to the wall. Further work needs to be done

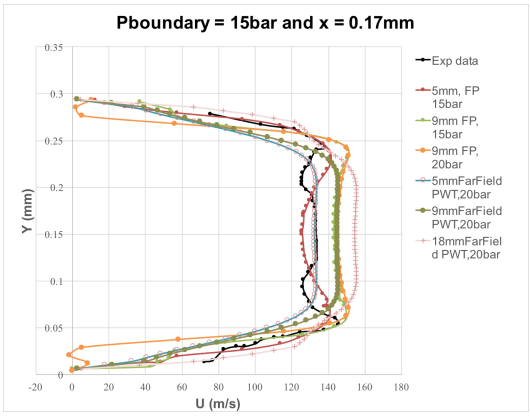

Figure 6. Spanwise Velocity plots at x=.17mm comparing experimental data at 15bar to various downstream pressure values

in order to confirm the stability of the wave transmissive boundary with regards to vapour formation in the far field.

References

[1] Anon. BS EN590:2013, 2013.

[2] R. Arndt. *Annual Review of Fluid Mechanics*, pages 273–328, 1981.

[3] R. Arndt. *Annual Review of Fluid Mechanics*, page 175, 2002.

[4] A. Bergant, R. Simpson, and S. Tijsseling. *Journal of Fluids and Structures*, 22(2):135–171, feb 2006.

[5] M. S. Chung, S. B. Park, and H. K. Lee. *Journal of Sound and Vibration*, 276(1-2):13–26, 2004.

[6] N. Dumont, O. Simonin, and C. Habchi. *8th International conference on Liquid Atomisation and Spray systems*, 2000.

[7] C.P. Egerer, S. Hickel, S. J. Schmidt, and N. Adams. *Physics of Fluids*, 26(8), 2014.

[8] Eric Goncalves and Regiane Fortes Patella. *Computers and Fluids*, 38(9):1682–1696, 2009.

[9] C. Habchi, N. Dumont, and O. Simonin. *Atomization and Sprays*, 18(2):129–162, 2008.

[10] C Habchi, FA Lafossas, P Beard, and D Broseta. *SAE paper 2004-01-1996*, 2004.

[11] C.W Hirt and B.D Nichols. *Journal of Computational Physics*, 39(1):201 – 225, 1981.

[12] Jean-Pierre Franc and Jean-Marie Michel. *Fundamentals of Cavitation*. Kluwer Academic Publishers, Dordrecht, 2004.

[13] F.P. Kärrholm. *Numerical modelling of diesel spray injection, turbulence interaction and combustion*. PhD thesis, Mech Eng, Goteborg, 2008.

[14] F.P. Kärrholm, H. Weller, and N. Nordin. *5th Joint ASME/JSME Fluids Engineering Conference*, pages 465–474, 2007.

[15] P. Koukouvinis, M. Gavaises, J. Li, and L. Wang. *Journal of Physics: Conference Series 9th International Symposium on Cavitation*, 656:012088, 2015.

[16] X. Margot, S. Hoyas, A. Gil, and S. Patouna. *Engineering Applications of Computational Fluid Mechanics*, 6(1):15–24, 2012.

[17] Sergey Martynov. *Analysis*, pages 1–226, 2005.

[18] Cyril Mauger, Loic Mees, Marc Michard, Alexandre Azouzi, and Stephane Valette. *Experiments in Fluids*, 53(6):1895–1913, 2012.

[19] F. Nicoud and F. Ducros. *Flow, Turbulence and Combustion*, 62(3):183–200, 1999.

[20] Stavroula Patouna. *A CFD STUDY OF CAVITATION IN REAL SIZE DIESEL INJECTORS*. PhD thesis, University Polytechnica Valencia, 2012.

[21] T.J. Poinsot and S.K Lele. *Journal of Computational Physics*, 99(2):352, apr 1992.

[22] Tao Qiu, Xin Song, Yan Lei, Xinghua Liu, Xiaodong An, and Mingchia Lai. *Applied Thermal Engineering*, 109:364–372, 2016.

[23] F. Ruiz and L. He. *Atomization and Sprays*, 9:419–429, 1999.

[24] Kaushik Saha, Ehab Abu-Ramadan, and Xianguo Li. *Journal of Engineering for Gas Turbines and Power*, 135(6):062801, 2013.

[25] F. J. Salvador, J. V. Romero, M. D. Roselló, and J. Martínez-López. *Mathematical and Computer Modelling*, 52(7-8):1123–1132, 2010.

[26] David P. Schmidt, Christopher J. Rutland, and Michael L. Corradini. *Atomization and Sprays*, 9(3):255–276, 1999.

[27] K. Vogiatzaki, P. Koukouvinis, and J. Carlton. *ILASS 2016*, pages 1–8, 2016.

[28] G. B. Wallis. *One-dimensional two-phase flow*. McGraw-Hill, 1969.

[29] Xiang Wang and WanHua Su. *Chinese Science Bulletin*, 54(10):1655–1662, may 2009.

[30] E. Winklhofer, E. Kelz, and A. Morozov. *Proceedings of the ILASS-Europe Conference, Sorrento*, 2003.

[31] E. Winklhofer, E. Kull, E. Kelz, and A. Morozov. *Proceedings of the ILASS-Europe Conference, Zurich*, page 574 ? 579, 2001.